J. Fluid Mech. (1971), *vol.* 45, *part* 2, *pp.* 341–351
Printed in Great Britain

Instability and secondary motion in a rotating channel flow

By JOHN E. HART†

Department of Meteorology, M.I.T.

(Received 22 July 1969 and in revised form 9 June 1970)

An experiment with the pressure-driven flow down a long rotating channel is described. For zero rotation the flow is quasi-parabolic, laminar, and one-dimensional up the channel. With slight rotation Ω there is a weak double-vortex secondary circulation aligned with the channel. At intermediate Ω there exists an instability in the form of longitudinal rolls of non-dimensional wave-number 5. The instability disappears at high rotation rates.

The general stability problem for a rotating zonal flow $\overline{U}(y)$ is considered theoretically. For perturbations independent of the co-ordinate in the direction of the flow, the problem is exactly analogous to the stability problem of a temperature-stratified fluid where the stratification $\overline{T}_z(z)$ corresponds to the quantity

$$(\partial \overline{U}/\partial y)\,(1/2\Omega) - 1.$$

This analogy extends to much more general mean fields (e.g. non-linear or time dependent) than does the oft-quoted analogy between thermal convection and cylindrical Couette flow. The instability theory is in qualitative agreement with the experiment.

1. Description of the experiment

Experiments with rotating fluids have usually been performed with cylindrical containers. The rotating annulus and the cylindrical Couette flow experiments are well known examples. These include, among many other things, experiments with source-sink flows (e.g. Hide 1968). However, most of these experiments are concerned with high rotation rates. It is the purpose of this paper to describe the flow régimes which occur as a rectangular channel flow is subjected to rotation.

The basic experimental device shown in figure 1 was a rectangular water tunnel, constructed out of plexiglass, with dimensions 90 cm long by 8 cm high by 1·15 cm deep. The channel was closed except for two chimneys, one at each end. Circulation was driven by establishing a constant pressure head across the two chimneys, the head being maintained by a small submersible pump. The flow was baffled at each end with 3 cm wide pieces of porous polyurethane foam (shaded regions in the figure) in the entrance and exit sections. The whole apparatus with a small reservoir containing the pump was placed on a rotating table. Different height taps on the chimneys provided a means for regulating

† Present address: D.A.M.T.P., Cambridge University.

the pressure head. Visualization was achieved by setting a group of fine horizontal and vertical wires in the tank and electrically stimulating a pH transition in a titrated solution of thymol blue indicator, a method which has been discussed in detail by Baker (1966).

The simple tunnel performed very well over a wide range of Ω (0 to 6 radian/sec) and an intermediate range of velocities (mean stream speed 0·5 to 2 cm/sec). For these experimental conditions the flow did not exhibit any instability due to end effects. For a central section of the tank about 20 cm from the entrance to 5 cm from the exit baffle, the flow was completely steady and parallel except for the motions discussed in the following sections. If the flow was driven much faster than 2 cm/sec eddies from the corner regions penetrated upstream.

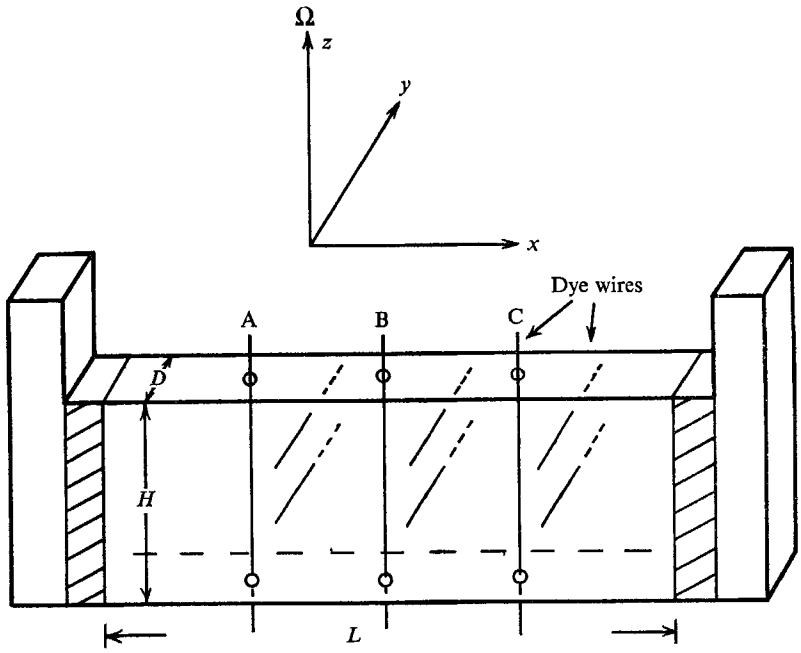

FIGURE 1. Schematic of the channel. Fluid flow is from left to right. The dye wire observation stations A, B, and C are at 0·25L, 0·5L and 0·75L respectively.

2. Experimental observations

We wish to discuss the results in terms of a velocity scale U, which is determined experimentally as the peak stream speed at dye station C. The length scale is taken as the channel width D. The flow is pressure driven so that the stream speed U is related to the pressure head Δp. The exact relationship will depend on the dynamics of the flow in the channel and in the corners, and on the drag in the baffles. Thus, it is more convenient to take the measured speed U as defining the system. Asymptotically far from the ends the flows will be independent of x (there are no observed transverse waves), so we can write a non-dimensional pressure $p = -Cx + P(y, z)$ where $P_{\text{dim}} = (\rho_0 U\nu/D)p$. C is the constant which relates the stream speed to the pressure head.

With the above assumptions the non-dimensional equations of steady motion in co-ordinates rotating with the channel are

$$R_e[vu_y + wu_z] - (1/E)\, v = C + [u_{yy} + u_{zz}], \tag{2.1}$$

$$R_e[vv_y + wv_z] + (1/E)\, u = -P_y + [v_{yy} + v_{zz}], \tag{2.2}$$

$$R_e[vw_y + ww_z] = -P_z + [w_{yy} + w_{zz}], \tag{2.3}$$

$$v_y + w_z = 0, \tag{2.4}$$

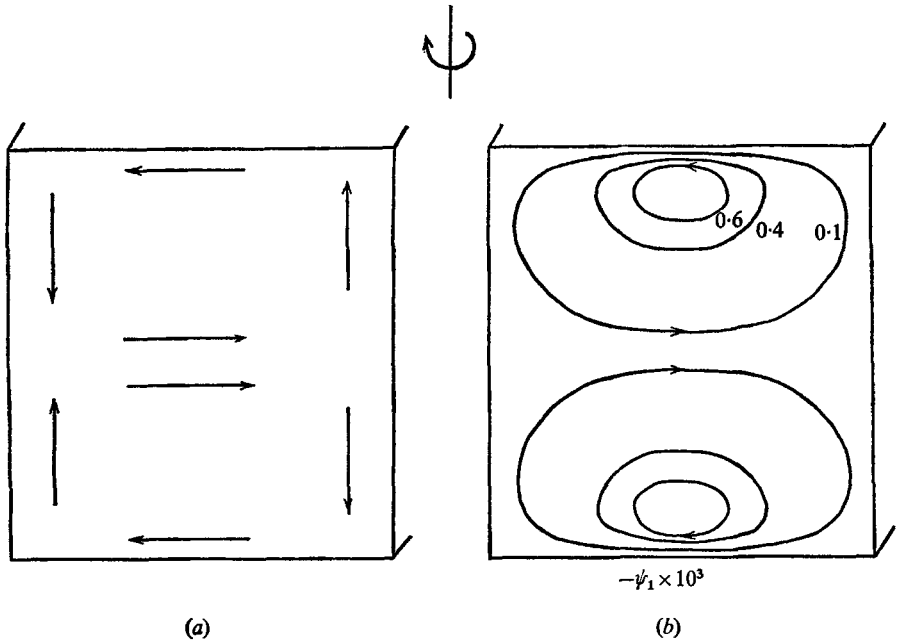

FIGURE 3. (*a*) shows the direction of the secondary circulation looking upstream; (*b*) contains the theoretical streamlines.

where the parameters are

$$R_e = UD/\nu,$$

$$E = \nu/fD^2.$$

Here, ν is the kinematic viscosity and $f = 2\Omega$. An additional parameter of interest is the Rossby number $R_o = R_e.E$.

The experiments were performed by establishing a steady flow at $f = 0$ and then slowly increasing the rotation. The following discussion concerns only the aforementioned central section.

For zero rotation the velocity has only a u component and is a function of y and z alone. Looking down on a horizontally injected dye line (from the same angle as the sketch in figure 1) we see from figure 2(*a*) (plate 1) that the flow is quasi-parabolic in y. In figure 2(*b*) we look in along the axis of the wire and see that the horizontal dye lines remain flat, evidence of the absence of vertical velocity for $f = 0$. The rotation was increased in a clockwise sense from zero. Immediately evident at even slight rotations was a weak secondary double

roll circulation. The vertical velocities are seen to lift dye lines out of horizontal planes (figure 2(*c*) and (*d*)). The two horizontal wires have been alternately pulsed, with equal time intervals. Their vertical positions are $-0{\cdot}12H$ and $0{\cdot}23H$ from the centreline $z = 0$, so that the upper probe is closer to a boundary. The sense of the secondary circulation is shown in figure 3(*a*). Figure 3(*b*) contains a streamline pattern calculated in §3. The increased secondary motion at the probe position closer to the boundary is reproduced in the theoretical solution which concentrates vorticity near the top and bottom walls.

The secondary motion is due to the vertical Coriolis torque u_z. This torque will generate $\hat{x}$-vorticity which accounts for the lifting of the dye lines observed in the photographs. Benton (1956) discussed this type of Coriolis-driven secondary motion in terms of the flow in a rotating pipe, where the rotation was to be that of the earth itself. Because the Rossby number for the earth's rotation and laboratory scales is so large, he was unable to observe this secondary motion directly.

In figure 4 we have made tracings from the photographs of vertical dye columns induced at dye wire C, figure 1. The straight line is the vertical wire, and each curved line to the right indicates the leading edge of a dye pulse. Figure 5 (plate 2) shows some photographs of the vertical streaks. In figure 4(*a*) we show the zero rotation profile. Figure 4(*b*) indicates there is a slight straightening of the interior part of the profile with the z variations moving nearer the boundaries. In 4(*e*) we see that the characteristic Taylor–Proudman interior flow has developed in which $\partial u/\partial z = 0$. It is the development of the secondary motion with Ω that leads to this régime. At very large rotation (small E, R_o) the secondary motion can be thought of as deriving from Ekman suction. Indeed the overshoot in figure 4(*e*) is roughly at the distance $z_{\text{dim}} = 2E^{\frac{1}{2}}D$ from the wall, which is the position of overshoot obtained from the theory of the linear Ekman layer. The strong rotation pipe flow has been studied by Benton & Boyer (1966). Their theoretical analysis does not strictly apply to the square channel and the boundary-layer methods described in Greenspan (1968) might be more useful in our geometry.

Although the secondary circulation is the first consequence of rotation, at intermediate values of R_o and E there is a second transition to a higher wave-number régime. The vertical dye lines in figures 4(*c*) and 4(*d*) indicate the appearance of a multiple x-independent roll structure of non-dimensional wave-number ~ 5. The onset is observed to take place when the mean flow is only slightly modified by the secondary motion (see figures 6 and 7). The rolls were detected by observing waviness in the vertical dye lines, waviness resulting from modification to the mean flow by the perturbations. We plot the observed states as a function of R_o and E^{-2} in figure 7.

On the basis of the stability analysis of §§4 and 5, it is thought that these higher wave-number motions are a true instability of the shear flow $\overline{U}(y, z)$. Basically the instabilities are quite similar to the well-known Taylor vortices, although the formulation perhaps has more in common with the meteorologists' long-standing concepts of dynamic stability (Solberg 1936). These all possess a 'circulation squared' type of necessary condition, which in the present case is

shown to be $R_o.\overline{U}_y - 1 > 0$. The solid curve of figure 7 is from the analysis. The instability theory predicts the states of the experiments rather well, especially the cut-offs at low R_o and low E^{-2}. The Coriolis force must be strong relative to viscosity, but not so strong as to completely dominate inertial effects.

As the rotation rate is further increased, the higher wave-number régime is stabilized and the fluid passes into the Taylor–Proudman type régime with $\partial\overline{U}/\partial z$ equal to zero in the interior (figure 4(*e*)). This transition involves the violation of the above necessary condition for instability, along with the effects of the continuous modification of the base flow.

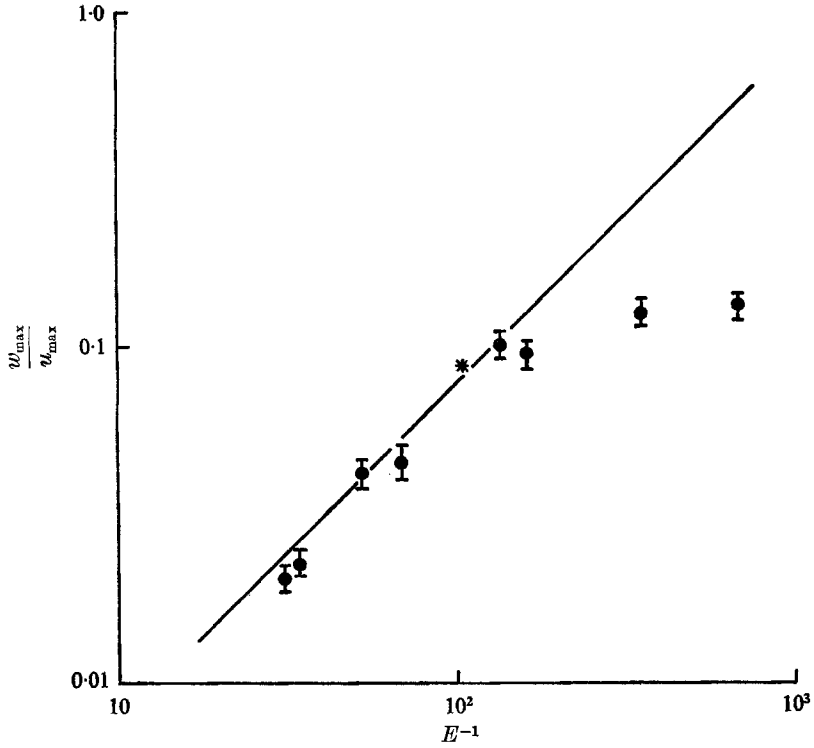

FIGURE 6. Experimental points of the ratio of the maximum secondary vertical velocity to the peak streamwise component. The solid line is from the theory and the star denotes an estimate of the upper limit of its validity.

In summary, as the channel flow is subjected to increasing rotation the motions pass through a succession of régimes: stable parabolic, to parabolic modified by secondary motion, to axisymmetric rolls, to stable Taylor–Proudman. The following sections look at some of these régimes theoretically.

3. Theoretical discussion of the secondary circulation

Benton (1956) has discussed the secondary circulation in a weakly rotating pipe flow. He basically considers a perturbation expansion valid as Ω goes to zero. We expect that a similar approach should be valuable in our rectangular

channel. In a sufficiently long channel the secondary motions should be independent of x. Equations (2.1)–(2.4) can then be written as a u momentum and as a streamwise vorticity equation,

$$R_e[\psi_z u_y - \psi_y u_z] - (1/E)\psi_z = C + u_{yy} + u_{zz}, \tag{3.1}$$

and

$$R_e[\psi_z \nabla^2\psi_y - \psi_y \nabla^2\psi_z] + (1/E)\, u_z = \nabla^4\psi, \tag{3.2}$$

where

$$v = \psi_z, \quad w = -\psi_y,$$

and

$$u = \psi_y = \psi_z = 0 \quad \text{on} \quad y = \pm\tfrac{1}{2}, \quad z = \pm H/2D.$$

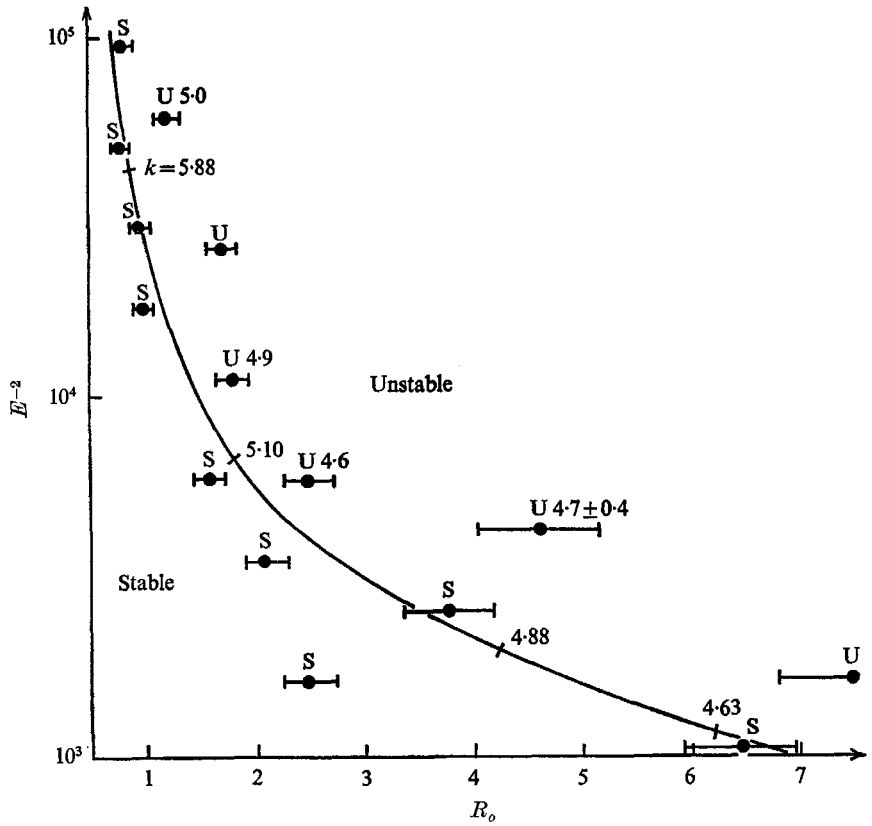

FIGURE 7. The points and error bars represent the observed experimental states. 'U' denotes an unstable state, and 'S' a stable one. The numbers are the vertical wavenumbers. The solid line is a theoretical curve from the theory for the neutral stability of the profile $\bar{U}(y) = 1 - 4y^2$, subject to viscous and Coriolis forces.

We expand

$$u = \sum_{n=0}^{\infty} (1/E^n)\, u_n, \tag{3.3}$$

and

$$\psi = \sum_{n=0}^{\infty} (1/E^n)\, \psi_n. \tag{3.4}$$

Equating like powers of E in (3.1) to (3.4) we obtain for $n = 0$

$$R_e[\psi_{0z} u_{0y} - \psi_{0x} u_{0z}] = C + u_{0yy} + u_{0zz}, \tag{3.5}$$

$$R_e[\psi_{0z} \nabla^2\psi_{0y} - \psi_{0y} \nabla^2\psi_{0z}] = \nabla^4\psi_0. \tag{3.6}$$

Subject to the boundary conditions the solutions are

$$\psi_0 \equiv 0 \tag{3.7}$$

and
$$u_0 = C\left[\frac{1}{8} - \frac{y^2}{2} - \frac{4}{\pi^3}\sum_{p=0}^{\infty} \frac{(-1)^p}{(2p+1)^3} \frac{\cosh(2p+1)\pi z \,.\cos(2p+1)\pi y}{\cosh(2p+1)\pi H/D}\right]. \tag{3.8}$$

With $n = 1$:

$$R_e[\psi_{1z} u_{0y} - \psi_{1y} u_{0z}] = u_{1yy} + u_{1zz}, \tag{3.9}$$

$$\nabla^4 \psi_1 = u_{0z}. \tag{3.10}$$

From (3.10) the mechanism for the secondary circulation is clear. It is driven by the differential Coriolis force u_{0z} which exists for arbitrarily small rotation as long as $u_{0z} \neq 0$. If there are rigid stationary horizontal boundaries this must be true somewhere in the flow.

Once we solve (3.10) we can go back to find u_1. The solution for ψ_1 is found by setting $z' = z\bar{h}$, where $\bar{h} = D/H$, and writing

$$\psi_1 = \sum_{i=1}^{N}\sum_{j=1}^{Q} A_{ij} C_i(y) S_j(z'), \tag{3.11}$$

where C_i and S_j are the orthonormal functions of Harris & Reid (1958), which satisfy all the boundary conditions on ψ (see also Chandrasekhar 1961*b*). The coefficients are found by requiring the error in (3.10) to be orthogonal to all the trial functions of (3.11). This leads to a set of linear equations which can be solved by matrix methods. We have solved this problem for $\bar{h} = 0{\cdot}143$, with $N = 5$ and $Q = 16$. The streamlines are shown in figure 3(*b*). This solution may be expected to be accurate only for sufficiently large E. If we require the correction to u_0 to be small we find that we must have $R_e . D/EH \ll 10^3$. Benton obtained exactly the same criterion for the rotating pipe. Even for equality in the above expression the $n = 1$ solutions are quite small. Indeed the secondary flows are very weak and for low Reynolds numbers rotation must be very large before the basic profile changes very much, at least in the interior. In our experiments where $R_e D/H \sim O(10)$, E should be greater than 10^{-2} for u_0 to be essentially unchanged by the $n = 1$ solution.

Since we were unable to look directly up the channel (because of the baffles), comparison with the theory was only possible by measuring the ratio of the maximum secondary vertical velocity to the peak upstream velocity from the side view dye streaks as in figure 2 (plate 1). This yields a comparison to the theory at the dye wire height z_0. The results are shown in figure 6. The agreement between theory and the limited experimental data is quite good, for $E \gtrsim 10^{-2}$.

4. Roll instabilities in a rotating shear flow

Basic equations

We now consider the stability of a flow between two vertical walls at $y = \pm \frac{1}{2}$. The equations of motion can be rewritten slightly as

$$R_o[\partial \mathbf{V}/\partial t + \mathbf{V} . \nabla \mathbf{V}] + \hat{k} \times \mathbf{V} = -\nabla p + E\nabla^2 \mathbf{V} \tag{4.1}$$

and
$$\nabla . \mathbf{V} = 0. \tag{4.2}$$

We further wish to study a mean flow similar to that in the experiment. The experimental flow (see (3.8)) varies with z and is modified by the secondary motion. However, from the experimental results, and from the theory of §3, there is good reason to suppose that a simpler expression for the mean stream velocity distribution will give useful theoretical stability results which should be applicable to the experimental data. We note that if $D/H \ll 1$ the z variations in the mean profile $\overline{U}(y,z)$ will be concentrated near the horizontal boundaries. Further, both the theory of §3, and that of Benton suggest that the secondary flow will give a small correction ($< 10\,\%$) to $\overline{U}$ if $R_o D/E^2 H \ll 10^3$. The measurements confirm this theoretical estimate. An independent estimate of corrections to $\overline{U}$ can be made by noting that in the high rotation régime $E^{\frac{1}{4}}$ sidewall layers will probably be important. We suppose that this régime will tend to a viscous régime as the $E^{\frac{1}{4}}$ layers fill the gap. On this basis we expect that viscosity will dominate over rotation throughout most of the channel provided $E^{-2} < 10^2$ to 10^3. This is roughly the same as our previous estimate with $R_o \sim 1$, $D/H \sim 0{\cdot}1$. So for $D/H \ll 1$ and $R_o D/E^2 H \ll 10^3$ we assume we can approximate the flow in the region away from the horizontal boundaries by

$$\overline{U} = 1 - 4y^2. \tag{4.3}$$

This is one of a class of exact solutions to the full equations (4.1) and (4.2) in which $\mathbf{V} = (U(y), 0, 0)$. These solutions must satisfy

$$\overline{U}(y) = -\overline{P}_y, \tag{4.4}$$

$$\overline{U}_{yy} = E^{-1}\overline{P}_x, \tag{4.5}$$

which are solved by

$$\overline{U} = (\overline{P}_x y^2/2E) + by + c, \tag{4.6}$$

$$\overline{P} = \overline{P}_x . x - (\overline{P}_x . y^3/6E) - \tfrac{1}{2}by^2 - cy, \tag{4.7}$$

where $\overline{P}_x$, b, and c are constants. The study of the stability of solutions with the form of (4.6) is of theoretical interest since these solutions do satisfy the full non-linear governing equations, and as we have noted, the stability of the particular solution (4.3) should be relevant to the experiment provided the parameters are in the range described above. In the usual manner we expand the dependent variables in terms of small perturbations on the mean fields (4.6) and (4.7). We find

$$R_o(u_t + \overline{U}u_x + v\overline{U}_y) - v = -p_x + E\nabla^2 u, \tag{4.8a}$$

$$R_o(v_t + \overline{U}v_x) + u = -p_y + E\nabla^2 v, \tag{4.8b}$$

$$R_o(w_t + \overline{U}w_x) = -p_z + E\nabla^2 w, \tag{4.8c}$$

$$u_x + v_y + w_z = 0. \tag{4.9}$$

In view of the experiment we consider here perturbations with $\partial/\partial x = 0$. Thus with $v = \psi_z$ and $w = -\psi_y$ we obtain

$$(E\nabla^2 - R_o\,\partial/\partial t)\,\nabla^2\psi = u_z \tag{4.10}$$

and

$$(E\nabla^2 - R_o\,\partial/\partial t)\,u = (R_o\overline{U}_y - 1)\,\psi_z. \tag{4.11}$$

If we separate the time and z dependence of the perturbations by introducing

$$\psi = \mathrm{Re}\{ie^{\sigma t}\, e^{ikz}\, h(y)\} \tag{4.12a}$$

and

$$u = \mathrm{Re}\{e^{\sigma t}\, e^{ikz}\, g(y)\} \tag{4.12b}$$

we obtain:

$$[E(d^2-k^2)-R_o\sigma]\,(d^2-k^2)\,h-kg=0, \tag{4.13}$$

$$[E(d^2-k^2)-R_o\sigma]\,g+(R_o\overline{U}_y-1)\,kh=0, \tag{4.14}$$

where $d \equiv d/dy$. The instability described here takes the form of periodic disturbances with axes parallel to the mean velocity and with vertical wavelengths $2\pi/k$. Solutions to (4.13) and (4.14) will be sought which satisfy rigid boundary conditions $h = dh = g = 0$ at $y = \pm\frac{1}{2}$.

Analogue to thermal instability

We shall now show that the linearized longitudinal instabilities of the rotating channel flow are dynamically equivalent to similar instabilities in a fluid contained between two horizontal differentially heated plates. Actually we shall demonstrate the analogy only for marginal stability, assuming $\sigma = 0$. The correspondence continues to hold for the general case with non-zero growth rates provided the Prandtl number of the thermally driven fluid is equal to one. Note that equations (4.13) and (4.14) with $\sigma = 0$ are exactly analogous to those obtained for the thermal problem by Pellew & Southwell (1940). Define a correspondence

$$kh/E \leftrightarrow W, \tag{4.15a}$$

$$g \leftrightarrow \theta, \tag{4.15b}$$

$$E^{-2} \leftrightarrow R_a, \tag{4.15c}$$

$$y \leftrightarrow z, \tag{4.15d}$$

$$R_o U_y - 1 \leftrightarrow -T_z. \tag{4.15e}$$

Using this, (4.13) and (4.14) are transformed into

$$(d^2-k^2)^2\, W = \theta \tag{4.16}$$

and

$$(d^2-k^2)\,\theta - R_a k^2 \overline{T}_z\, W = 0, \tag{4.17}$$

which are just the thermal instability equations mentioned above. Equation (4.16) like (4.13) gives the vorticity balance. Since the rotating flow and the stratified fluid instabilities are governed by the same equations and boundary conditions, results from the thermal problem can be applied here. For example, the necessary criterion for instability that the thermal gradient be negative somewhere in the interval between the boundaries is equivalent to requiring that $R_o\overline{U}_y > 1$ somewhere. The total vorticity must be negative in order that perturbations be regenerated by the coupling between the vorticity field and the Coriolis body force. This is identical to an inviscid condition long recognized by meterorologists (e.g. Solberg 1936, pp. 66–82) in the context of the 'inertial' stability of the jet streams. By use of (4.16) we can interchange eigenvalues and eigenfunctions for particular problems satisfying (4.15e). The most familiar

cases are where $\overline{T}$ is linear in z (conduction solution) or where $\overline{T}$ is parabolic (conduction with internal heat generation).

Debler (1966) has pointed out the analogy between the thermal problem (4.16) and (4.17) and the instability problem for cylindrical Couette flow. For certain $\overline{T}_z(z)$ the analogy is valid since the cylinder flow equations are, from Debler,

$$(d^2-k^2)^2 W = (1+\alpha' y)\theta, \tag{4.18}$$

$$(d^2-k^2)\theta = -\lambda W, \tag{4.19}$$

here λ is the eigenvalue, α' is the mean shear, and y is the independent (radial) variable. Chandrasekhar (1961*a*) has shown that the eigenvalues of the two systems (4.16)–(4.17) and (4.18)–(4.19) are identical, but it is clear that the eignenfunctions will not generally be the same since the mean field occurs in the vorticity equation in the cylinder problem and in the thermal equation in the stratified problem. However, the present analogy is exact.†

5. Solutions to the stability equations

The linear profile

We return to equations (4.13) and (4.14) and study solutions with $\sigma = 0$. We set $\overline{U}_y = 1$ (plane Couette flow), and write $H = (R_o - 1)/E^2$. The governing equation is easily seen to be $(d^2-k^2)^2(d^2-k^2)h + Hk^2h = 0$. Using the analogy to the thermal problem we have $H_{\text{critical}} = 1708$. This solution reaffirms the necessary condition $R_o \overline{U}_y > 1$.

Solution for the parabolic profile

We now consider $\overline{U} = 1-4y^2$. As already mentioned this is an approximation to the actual laboratory profile of § 2. It has no z dependence and hence does not allow a secondary circulation, but it should model the actual profile near $z = 0$. We have solved the stability equations numerically using the Galerkin method. This technique has been discussed in detail by Mikhlin (1964, pp. 448–91) and has been used in many hydrodynamic stability problems. The theoretical results are contained in the solid curve of figure 7. For decreasing R_o the critical parameter E^{-2} increases rapidly. From the necessary condition we expect that the curve should asymptotically approach $R_o = \frac{1}{4}$. Numerically we have found that for $R_o = \frac{1}{4}$ there are at least no eigenvalues below $E^{-2} = 10^7$. In terms of the thermal analogue this is because we have a series of distributions in temperature with a stable layer over an unstable one where the depth of the unstable layer decreases with decreasing R_o. For $R_o < \frac{1}{4}$ the stratification is completely stable. It is noted that in some cases the experimentally stable states lie in the unstable region. This is probably attributable to the rather insensitive method of observing

† The exact correspondence is further evidence of the well-known analogy between two-dimensional rotating and stratified fluids. The mechanism for the rotating channel instability is similar to that for Taylor vortices in that the inviscid condition $R_o \overline{U}_y > 1$ can be shown to be equivalent to the condition of Rayleigh that the square of the circulation decrease outward (for this purpose the channel must be placed at an infinite radius). However, there is no limiting process which transforms the general cylindrical Couette flow instability problem into the thermal instability problem.

the onset of the small amplitude instabilities. Also for the part of the curve with $E^{-2} > 10^4$ the simple mean field of (4.3) is probably not entirely accurate with regard to the experiment. However, the generally favourable comparison with the laboratory data suggests that the observed wavy structure in the vertical dye lines is indeed amenable to interpretation as due to a Coriolis-driven instability of the horizontal shear flow.

6. Summary and conclusions

A simple experiment with a rotating channel flow has been described. The motions induced by rotation are (i) a weak secondary double roll flow which depends on non-zero u_z for its existence, and (ii) a roll instability depending on non-zero u_y. Further quantitative studies should perhaps concentrate on one or the other of these flows, which means using either a square, or a tall narrow channel.

It has been shown that longitudinal roll instabilities of a rotating zonal flow are identical to two-dimensional roll instabilities in a thermally stratified fluid provided $\overline{T}_z(z)$ has the functional form $1 - R_o.\overline{U}_y(y)$. Conclusions reached from the study of the rotating system carry over to the stratified fluid problem, and *vice versa*.

I would like to thank Prof. R. Beardsley of M.I.T. for generously offering the use of his rotating table for the experiments.

The research was sponsored under the A.F.O.S.R. under contract AF 49-638-1493. The numerical calculations were carried out at the M.I.T. computation centre.

REFERENCES

BAKER, D. J. 1966 A technique for precise measurement of small fluid velocities. *J. Fluid Mech.* **26**, 573.

BENTON, G. S. 1956 The effects of the earth's rotation on laminar flow in pipes. *J. Appl. Mech.* **23**, 123–127.

BENTON, G. S. & BOYER, D. 1966 Flow through a rapidly rotating conduit of arbitrary cross-section. *J. Fluid Mech.* **26**, 69.

CHANDRASEKHAR, S. 1961*a* Adjoint differential systems in the theory of hydrodynamic stability. *J. Math. Mech.* **10**, 683.

CHANDRASEKHAR, S. 1961*b* *Hydrodynamic and Hydromagnetic Stability*. Oxford University Press.

DEBLER, W. R. 1966 On the analogy between thermal and rotational hydrodynamic stability. *J. Fluid Mech.* **24**, 165–176.

GREENSPAN, H. P. 1968 *The Theory of Rotating Fluids*. Cambridge University Press.

HARRIS, D. L. & REID, W. H. 1958 On orthogonal functions which satisfy four boundary conditions. *Astrophys. J. Supp. Ser.* **3**, 429–447.

HIDE, R. 1968 On source-sink flows in a rotating fluid. *J. Fluid Mech.* **32**, 737–764.

MIKHLIN, S. G. 1964 *Variational Methods in Mathematical Physics*. Pergamon.

PELLEW, A. & SOUTHWELL, R. V. 1940 On maintained convective motion in a fluid heated from below. *Proc. Roy. Soc.* A **176**, 312–343.

SOLBERG, H. 1936 *Procés Verbaux Météorol., Union Géod. Géophys. Intern. II*. Edinburgh.

FIGURE 2. Typical patterns from the horizontal wires. In (*a*) we look down on a horizontal wire and see the quasi-parabolic y dependence on the channel flow obtained with $f = 0$. The stream speed is 2·2 cm/sec. (*b*) is a side view of the same situation and shows the absence of vertical velocities. As the channel is spun up a secondary motion is evident as the vertical velocity tips the dye lines out of horizontal planes. For (*c*), $R_o = 3{\cdot}6$, $E^{-1} = 4{\cdot}2 \times 10$. For (*d*), $R_o = 1{\cdot}2$, $E^{-1} = 1{\cdot}28 \times 10^2$.

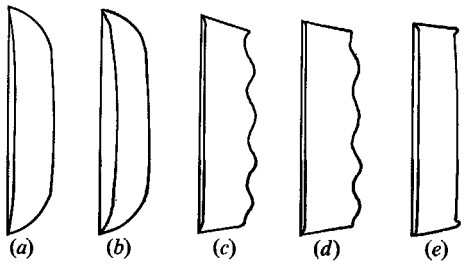

FIGURE 4. Tracings of the development of dye lines induced from the vertical wire at station C. As f increases there is a general sharpening of the profile. For intermediate f, a higher mode is evident. (*a*) $\Omega = 0$; (*b*) $R_o = 6{\cdot}5$, $E^{-2} = 936$; (*c*) $R_o = 2{\cdot}6$, $E^{-2} = 6200$; (*d*) $R_o = 1{\cdot}8$, $E^{-2} = 1{\cdot}10 \times 10^4$; (*e*) $R_o = 0{\cdot}44$, $E^{-2} = 3{\cdot}47 \times 10^4$.

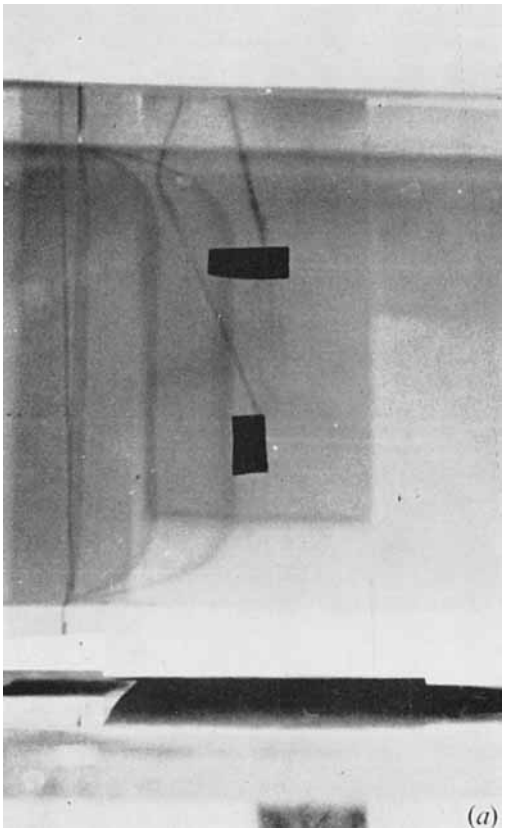

FIGURE 5. Typical photographs of vertically induced dye streaks. Cases (*a*)–(*c*) correspond to figures 4(*a*), 4(*d*) and 4(*e*) respectively.

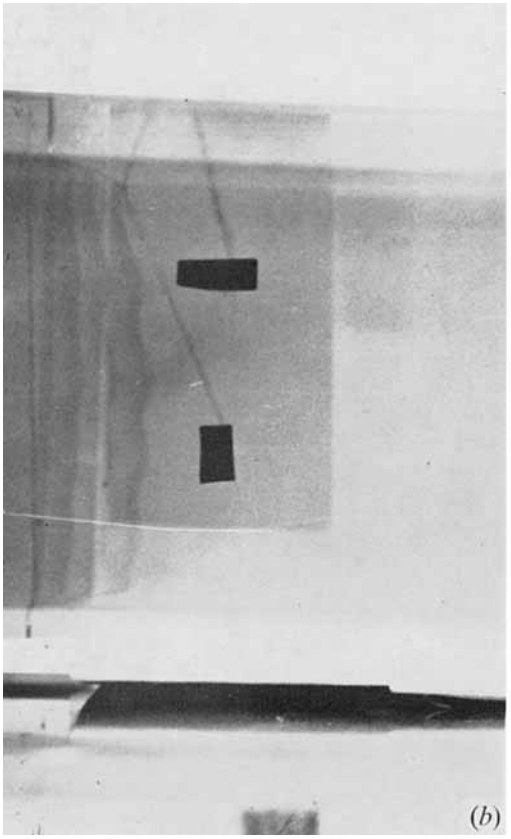

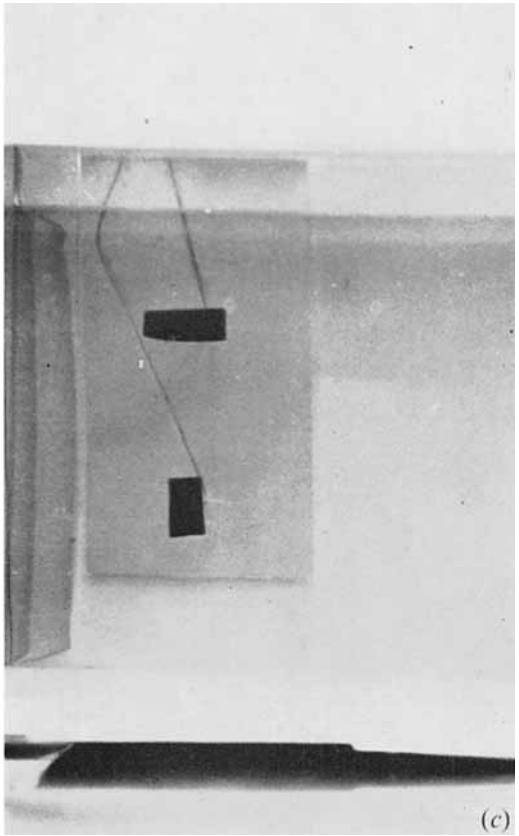

FIGURE 5. For legend see above.